Recoil-induced subradiance in an ultracold atomic gas

M. M. Cola, D. Bigerni, and N. Piovella
Dipartimento di Fisica, Università degli Studi di Milano and INFN Sezione di Milano, Via Celoria 16, Milano I-20133, Italy
(Received 7 February 2009; published 14 May 2009)

Subradiance, i.e., the cooperative inhibition of spontaneous emission by destructive interatomic interference, can be realized in a cold atomic sample confined in a ring cavity and lightened by a two-frequency laser. The atoms, scattering the photons of the two laser fields into the cavity mode, recoil and change their momentum. Under proper conditions the atomic initial momentum state and the first two momentum recoil states form a three-level degenerate cascade. A stationary subradiant state is obtained after the scattered photons have left the cavity, leaving the atoms in a coherent superposition of the three collective momentum states. Both a semiclassical description of the process and the quantum subradiant state with its Wigner function are given. Antibunching, quantum correlations, and entanglement between the atomic modes of the subradiant state are demonstrated.

DOI: 10.1103/PhysRevA.79.053622 PACS number(s): 03.75.−b, 42.50.Nn, 37.10.Vz

I. INTRODUCTION

Recent experiments with Bose-Einstein condensates (BECs) driven by a far-off-resonant laser beam have demonstrated collective super-radiant Rayleigh [1–4] and Raman scatterings [5,6], sharing strong analogies with the super-radiant emission from excited two-level atoms [7]. In these experiments an elongated BEC scatters the pump photons into the end-fire modes along the major dimensions of the condensate, acquiring a multiple of the two-photon recoil momentum $\hbar\vec{q}$, where $\vec{q}=\vec{k}-\vec{k}_s$ and $\vec{k}$ and $\vec{k}_s$ are the wave vectors of the pump and the scattered field. Theoretical works have shown that the super-radiant Rayleigh scattering relies on the quantum collective atomic recoil lasing (QCARL) gain mechanism, in which the fast escape of the emitted radiation from the atomic medium leads to the super-radiant emission [8–10]. The quantum regime of collective atomic recoil laser (CARL) [11,12] occurs when the two-photon recoil frequency $\omega_r=\hbar q^2/2M$ is larger than the gain bandwidth, such that the recoil frequency shifts the atoms out of resonance, inhibiting further scattering processes. As a consequence in the QCARL each atom coherently scatters a single pump photon, changing momentum by $\hbar q$. The process in which the atoms make a transition between two momentum states ($\vec{p}=\vec{0}$ and $\vec{p}=\hbar\vec{q}$) has strong analogies with that of two-level atoms prepared in the excited state and decaying to the lower state by spontaneous and stimulated emission. However, the incoherent spontaneous emission dominating the two-level atomic decay is absent in the momentum transition, where spontaneous emission is associated to momentum diffusion due to the scattering force, which can be made very small if the laser is sufficiently detuned from the atomic resonance. The absence of Doppler broadening and the long decoherence time of a BEC allow observation of super-radiance and coherent spontaneous emission from collective recoil much more easily than from electronic transitions in excited atoms, in which the decay is dominated by the incoherent spontaneous emission.

Another example of cooperative phenomenon from excited two-level atoms is subradiance, i.e., the cooperative inhibition of spontaneous emission by a destructive interatomic interference. This phenomenon, whose existence was proposed by Dicke [13] in 1954 in the same paper predicting super-radiance, has received less consideration than the more popular super-radiance, also due to the difficulty of its experimental observation. In fact, the only experimental proof was done in 1985 by Pavolini *et al.* [14]. Among different schemes of multilevel systems in which subradiance was predicted, Crubellier and co-workers [15–18], in a series of theoretical papers, proposed a three-level degenerate cascade configuration in which cooperative spontaneous emission is expected to exhibit new and striking subradiance effects.

In this paper we show that subradiance in a three-level degenerate cascade can be realized in a BEC inserted in a ring cavity and lightened by a two-frequency laser with frequency difference twice the two-photon recoil frequency, as illustrated in Fig. 1. The frequency of the scattered photon is determined by energy and momentum conservation. The process consists of two steps. In the first step the atoms initially at rest scatter the laser photons of frequency ω into the cavity mode of frequency $\omega_s=\omega-\omega_r$, changing momentum from 0 to $\vec{p}=\hbar\vec{q}$. In the second step the atoms scatter the laser photon of frequency $\omega+\Delta$, changing their momentum from $\vec{p}=\hbar\vec{q}$ to $\vec{p}'=2\hbar\vec{q}$. Since the change in the atomic kinetic energy is $\Delta E=(p'^2-p^2)/2M=3\hbar\omega_r$, by energy conservation the frequency of the scattered photon is $\omega+\Delta-3\omega_r$, which coincides with the frequency generated in the first step when $\Delta=2\omega_r$. In this way a three-momentum-level degenerate cascade is realized in which the atoms, initially with momentum $\vec{p}=\vec{0}$, change momentum to the intermediate value $\hbar\vec{q}$ and

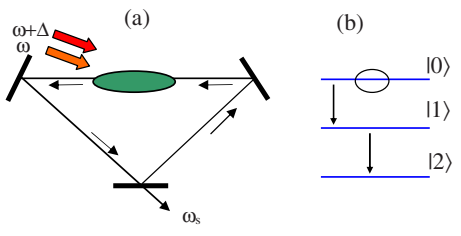

FIG. 1. (Color online) (a) Schematic diagram illustrating the geometry of a two-frequency pump CARL experiment; (b) three-level cascade scheme.

then to the final value $2\hbar\vec{q}$, emitting two degenerate photons of frequency $\omega_s=\omega-\omega_r$. In general the process, as described in Ref. [19], will continue with another scattering of the photon of frequency $\omega+\Delta$, changing the atomic momentum from $2\hbar\vec{q}$ to $3\hbar\vec{q}$ with the emission of a photon of frequency $\omega+\Delta-5\omega_r=\omega-3\omega_r$, and so on. However, if the cavity linewidth is much narrower than the frequency spacing, $\kappa \ll 2\omega_r$, these other frequencies will be damped out. Then, the oscillation of only the frequency $\omega_s=\omega-\omega_r$ in the cavity will restrict the momentum cascade to the three momentum states 0, $\hbar\vec{q}$, and $2\hbar\vec{q}$. A basic feature of this system is that the transition rates are proportional to the pump intensities, so that they can be varied with continuity. This makes the subradiance observation much easier than with a three-level cascade between electronic energy levels, where the transition rates are fixed by the branching ratios.

II. SEMICLASSICAL TREATMENT

A. General model

The QCARL with a two-frequency pump is described by the following equations for the order parameter $\Psi(z,t)$ of the matter field and the cavity-mode field amplitude $a(t)$ [19]:

$$i\frac{\partial\Psi}{\partial t}=-\frac{\hbar}{2m}\frac{\partial^2\Psi}{\partial z^2}+ig[\alpha(t)a^*e^{i(qz-\delta t)}-\text{c.c.}]\Psi, \tag{1}$$

$$\frac{da}{dt}=gN\alpha(t)\int dz|\Psi|^2e^{i(qz-\delta t)}-\kappa a, \tag{2}$$

where z is the coordinate along the cavity axis and t is the interaction time. The equations have been derived by performing the adiabatic elimination of the atomic internal degrees of freedom [8] but replacing the pump field with $E_p=e^{i(\vec{k}\cdot\vec{x}-\omega t)}(E_0+E_1e^{-i\Delta t})$: the pump laser has a sideband with frequency of $\omega+\Delta$, with $\Delta=2\omega_r$ [where $\omega_r=\hbar q^2/2M$ and $q=2k\sin(\phi/2)$], and electric field E_1. In Eqs. (1) and (2) $\alpha(t)=1+\epsilon\exp(-i\Delta t)$, where

$$\epsilon=\frac{E_1}{E_0} \tag{3}$$

is the two-pump field amplitude ratio. The other variables and parameters are $a(t)=(\epsilon_0V/2\hbar\omega_s)^{1/2}E_s(t)$, the dimensionless electric field amplitude of the scattered radiation beam with frequency ω_s; $g=(\Omega_0/2\Delta_0)(\omega d^2/2\hbar\epsilon_0V)^{1/2}$, the coupling constant; $\Omega_0=dE_0/\hbar$, the Rabi frequency of the pump laser incident with an angle ϕ with respect to the z axis ($\phi=\pi$ if counterpropagating), with electric field E_0 and frequency ω detuned from the atomic resonance frequency ω_0 by $\Delta_0=\omega-\omega_0$; $d=\hat{\epsilon}\cdot\vec{d}$, the electric dipole moment of the atom along the polarization direction $\hat{\epsilon}$ of the laser; V, the cavity-mode volume; N, the total number of atoms in the condensate; $\delta=\omega-\omega_s$, the pump-cavity detuning, and κ, the cavity linewidth. The emitted frequency ω_s is within the cavity frequency linewidth, whereas the pump field is external to the cavity so that its frequencies are not dependent on the cavity ones. The order parameter Ψ of the matter field is normalized such that $\int dz|\Psi|^2=1$.

If the condensate is much longer than the radiation wavelength and approximately homogeneous, then periodic boundary conditions can be applied on the atomic sample and the order parameter can be written as $\Psi(z,t)=\Sigma_nc_n(t)u_n(z)e^{-in\delta t}$, where $u_n(z)=(q/2\pi)^{1/2}\exp[in(qz)]$ are the momentum eigenstates with eigenvalues $p_z=n(\hbar q)$. Using this expansion, Eqs. (1) and (2) become

$$\frac{dc_m}{dt}=-i\omega_mc_m+g[\alpha(t)a^*c_{m-1}-\alpha^*(t)ac_{m+1}], \tag{4}$$

$$\frac{da}{dt}=gN\alpha(t)\sum_n c_mc_{m+1}^*-\kappa a, \tag{5}$$

where $\omega_n=n(n\omega_r-\delta)$.

B. Three-level approximation

As has been discussed elsewhere [8,20], if the gain rate is smaller than the recoil frequency the atoms recoil only along the positive direction of $\vec{q}$, absorbing a photon from the laser and emitting it into the cavity mode. Backward recoil, in which an atom absorbs a photon from the cavity mode and emits it into the laser mode, is inhibited by energy conservation. In this way, the laser photon of frequency ω induces a momentum transition from $m=0$ to $m=1$, emitting in the cavity a photon with frequency $\omega_s=\omega-\omega_r$. The laser photon of frequency $\omega+\Delta$ (with $\Delta=2\omega_r$) induces a momentum transition from $m=1$ and $m=2$, emitting another photon of the same frequency ω_s. If the cavity linewidth κ is smaller than $2\omega_r$, only the photons with frequency ω_s will survive in the cavity. Since further scattering would generate photons with frequencies $\omega-m\omega_r$, with $m=3,5,\ldots$, which cannot oscillate in the cavity, then the Hilbert space of the atoms is spanned by only the first three recoil momentum levels, $m=0,1,2$, and Eqs. (4) and (5) reduce to

$$\frac{dc_0}{dt}=-g\alpha^*(t)ac_1, \tag{6}$$

$$\frac{dc_1}{dt}=i(\delta-\omega_r)c_1+g[\alpha(t)a^*c_0-\alpha^*(t)ac_2], \tag{7}$$

$$\frac{dc_2}{dt}=2i(\delta-2\omega_r)c_2+g\alpha(t)a^*c_1, \tag{8}$$

$$\frac{da}{dt}=gN\alpha(t)(c_0c_1^*+c_1c_2^*)-\kappa a. \tag{9}$$

Equations (6)–(9) contain fast oscillating terms. They can be eliminated by introducing the slowly varying variable $\tilde{c}_2=c_2\exp(i\Delta t)$ and approximating Eqs. (6)–(9), neglecting the fast oscillating terms proportional to $\exp(\pm i\Delta t)$. In this way Eqs. (6)–(9) reduce to

$$\frac{dc_0}{dt}=-gac_1, \tag{10}$$

$$\frac{dc_1}{dt}=i(\delta-\omega_r)c_1+g(a^*c_0-\epsilon a\tilde{c}_2), \tag{11}$$

$$\frac{d\tilde{c}_2}{dt} = 2i(\delta - \omega_r)\tilde{c}_2 + g\epsilon a^* c_1, \tag{12}$$

$$\frac{da}{dt} = gN(c_0 c_1^* + \epsilon c_1 \tilde{c}_2^*) - \kappa a. \tag{13}$$

Equations (10)–(13) describe the three-level degenerate cascade of the atoms driven by two laser fields at frequencies ω and $\omega+2\omega_r$, respectively, and interacting with the self-generated cavity mode at the frequency $\omega_s=\omega-\omega_r$. Notice that the second transition rate, from $m=1$ to $m=2$, is proportional to the two-pump amplitude ratio ε.

C. Subradiance in three-level degenerate cascade

Asymptotically, in a time much longer than $1/\kappa$, the photons leave the cavity and the total polarization in Eq. (13) vanishes:

$$c_0 c_1^* + \epsilon c_1 \tilde{c}_2^* = 0. \tag{14}$$

On resonance ($\delta=\omega_r$) and with the atoms initially at rest [$c_0(0)=1$], the variables c_0, c_1, $\tilde{c}_2$, and a are real and Eqs. (10)–(13) keep invariant the following quantity [16]:

$$J = \epsilon^2 c_0^2 + \tilde{c}_2^2 + 2\epsilon c_0 \tilde{c}_2 = \epsilon^2. \tag{15}$$

From it we see that the atoms cannot populate completely the final state $m=2$ (with $\tilde{c}_2=1$ and $c_0=0$) unless the two-pump field amplitude ratio is $\epsilon=1$. Hence, when $\epsilon\neq 1$ the atoms remain in the intermediate levels $m=0$ and $m=1$ in a subradiant state. Condition (14), together with constraints (15) and the normalization $c_0^2+c_1^2+\tilde{c}_2^2=1$, determines univocally the steady-state solution reached asymptotically by the atoms. It is easy to show that for $\epsilon<1/\sqrt{3}$,

$$c_0 = -\epsilon\tilde{c}_2 = \frac{\epsilon^2}{1-\epsilon^2}, \quad c_1 = \left[1 - \frac{\epsilon^2(1+\epsilon^2)}{(1-\epsilon^2)^2}\right]^{1/2} \tag{16}$$

whereas for $\epsilon>1/\sqrt{3}$,

$$c_0 = \frac{1-\epsilon^2}{1+\epsilon^2}, \quad c_1 = 0, \quad \tilde{c}_2 = -\frac{2\epsilon}{1+\epsilon^2}. \tag{17}$$

Figure 2 shows the steady-state populations $P_i=|c_i|^2$ for $i=0,1,2$ plotted vs the two-pump field amplitude ratio ϵ. We observe that increasing ϵ from zero, the population of the intermediate state, P_1, decreases and the population of the final state, P_2, increases. They are equal for $\epsilon=1/2$, with $c_0=1/3$ and $c_1=-\tilde{c}_2=2/3$. The population of the initial state, P_0, increases too and reaches a local maximum for $\epsilon=1/\sqrt{3}$ with $c_0=1/2$, $c_1=0$, and $\tilde{c}_2=\sqrt{3}/2$. Then, for $\epsilon\geqslant 1/\sqrt{3}$ the intermediate state $m=1$ is empty ($c_1=0$) and the population of the initial state, P_0, decreases to zero for $1/\sqrt{3}<\epsilon\leqslant 1$. For $\epsilon>1$ it increases until it equals the population of the final state, P_2, when $\epsilon=1+\sqrt{2}$. For $\epsilon>1+\sqrt{2}$ the population of the initial state, P_0, is larger than that of the final state, P_2. However, this case appears stationary only because the semiclassical model neglects spontaneous emission. The quantum treatment, reported in Sec. III, shows that the stationary subradiant state may exist only for $0<\epsilon<1+\sqrt{2}$.

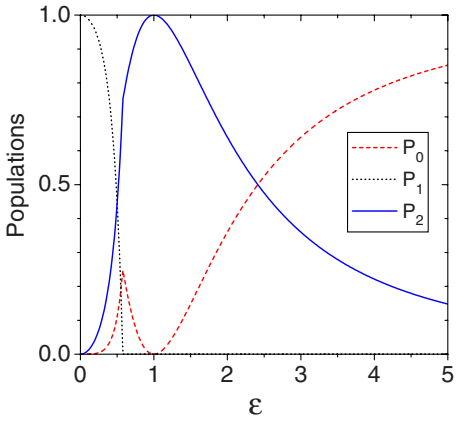

FIG. 2. (Color online) Semiclassical subradiance solution: populations of the three states, P_0 (dashed red line), P_1 (dotted gray line), and P_2 (continuous blue line) as functions of the two-pump field amplitude ratio ϵ, as given by Eqs. (16) and (17).

In order to illustrate how the system evolves toward the subradiance state, Fig. 3 shows the time evolution of the field $|a|^2$ [Fig. 3(a)], and the three populations [Fig. 3(b); P_0 (dashed blue line), P_1 (continuous red line), and P_2 (dashed-dotted black line)], obtained by solving the complete Eqs. (4) and (5) for $g\sqrt{N}=0.01\omega_r$, $\kappa=0.006\omega_r$, $\delta=\omega_r$, and $\epsilon=1/2$, with initial condition $c_0(0)=1$, $c_{i\neq 0}(0)=0$, and $a(0)=0.01$. The final populations are $P_0=1/9$ and $P_1=P_2=4/9$, according to Eq. (16).

In order to test the dependence of the subradiance state on the frequency difference Δ between the two pump fields, Fig. 4 shows the asymptotic coherence $C_{1,2}=|c_1 c_2^*|$ between the intermediate and the final states vs Δ for $g=0.01\omega_r$, $\delta=\omega_r$, $\epsilon=1/2$, and $\kappa=0.003\omega_r$ (dashed blue line), $\kappa=0.006\omega_r$ (dashed-dotted red line), and $\kappa=0.012\omega_r$ (continuous black line). The result shows that subradiance requires a very fine tuning of the pump frequency difference near $2\omega_r$, within a precision $\delta\omega\ll g\sqrt{N}$.

As a second example, Figs. 5 and 6 show the same case as in Figs. 3 and 4 but with $\epsilon=1+\sqrt{2}$. In this case $P_1=0$ and $P_0=P_2=1/2$. We note that whereas in the case $\epsilon=1/2$ the resonance linewidth in Fig. 4 decreases when the cavity loss κ increases, in the case $\epsilon=1+\sqrt{2}$ the linewidth increases with κ and it is about a factor of 100 larger. Hence the subradi-

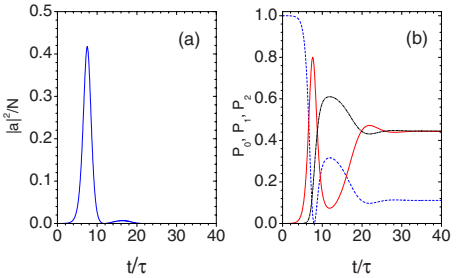

FIG. 3. (Color online) (a) Time evolution of the radiated intensity $|a|^2$ and (b) the three populations P_0 (dashed blue line), P_1 (continuous red line), and P_2 (dashed-dotted black line) vs t/τ, where $\tau=(g\sqrt{N})^{-1}$, for $g\sqrt{N}=0.01\omega_r$, $\kappa=0.006\omega_r$, $\delta=\omega_r$, and $\epsilon=1/2$.

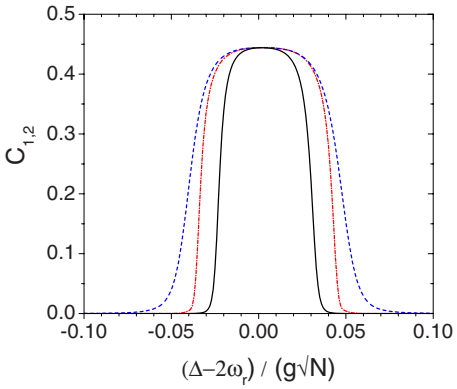

FIG. 4. (Color online) Asymptotic coherence $C_{1,2}=|c_1c_2^*|$ between the intermediate and the final states vs $(\Delta-2\omega_r)/g\sqrt{N}$ for $g=0.01\omega_r$, $\delta=\omega_r$, $\epsilon=1/2$, and $\kappa=0.003\omega_r$ (dashed blue line), $\kappa=0.006\omega_r$ (dashed-dotted red line), and $\kappa=0.012\omega_r$ (continuous black line).

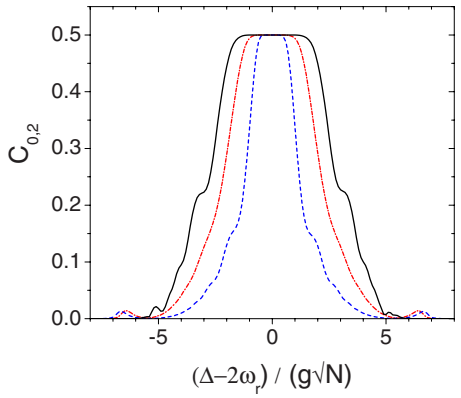

FIG. 6. (Color online) Asymptotic coherence $C_{0,2}=|c_0c_2^*|$ between the initial and the final states vs $(\Delta-2\omega_r)/g\sqrt{N}$ for $g=0.01\omega_r$, $\delta=\omega_r$, $\epsilon=1+\sqrt{2}$, and $\kappa=0.003\omega_r$ (dashed blue line), $\kappa=0.006\omega_r$ (dashed-dotted red line), and $\kappa=0.012\omega_r$ (continuous black line).

ance with $\epsilon=1/2$ is more sensible to the frequency mismatch than that with $\epsilon=1+\sqrt{2}$.

III. QUANTUM TREATMENT

A. Subradiant state

Let now obtain the subradiant state quantum mechanically, treating the amplitude c_n as bosonic operators $\hat{c}_n$ with commutation rules $[\hat{c}_m,\hat{c}_n^\dagger]=\delta_{m,n}$. Then, according to Eq. (14) the subradiant state $|\mathrm{sr}\rangle$ satisfies

$$(\hat{c}_0\hat{c}_1^\dagger+\epsilon\hat{c}_1\hat{c}_2^\dagger)|\mathrm{sr}\rangle=0 \tag{18}$$

(we omit the tilde on $\hat{c}_2$). It is possible to demonstrate (see Appendix A) that for a system of N atoms (with N even) there are $N/2$ subradiant states $|\mathrm{sr}\rangle_p$, with $p=1,2,\ldots,N/2$, defined as [16]

$$|\mathrm{sr}\rangle_p=C_p\sum_{k=0}^{p}\frac{(-1/2\epsilon)^k}{k!}\sqrt{\frac{(2k)!\,(N-p-k)!}{(p-k)!}}\times|p-k,2k,N-p-k\rangle, \tag{19}$$

where $|m,n,l\rangle=|m\rangle_0|n\rangle_1|l\rangle_2$ and C_p is a normalization constant. The index p is related to the population difference between the initial and final states, since $N_0-N_2=2p-N$. The case $p=0$ corresponds to the state $|0,0,N\rangle$. The link between the subradiant state $|\mathrm{sr}\rangle_p$ and semiclassical solutions (16) and (17) is provided by the correspondence between p and the population difference $N_0-N_2=N(c_0^2-c_2^2)$ in the limit $N\gg1$. For $\epsilon<1/\sqrt{3}$, $p=(N/2)(1-2\epsilon^2)/(1-\epsilon^2)$ and for $\epsilon>1/\sqrt{3}$, $p=N[1-4\epsilon^2/(1+\epsilon^2)^2]$. As particular cases, $p=N/3$ for $\epsilon=1/2$ and $p=N/4$ for $\epsilon=1/\sqrt{3}$. Furthermore, $p=0$ for $\epsilon=1$ and $p=N/2$ for $\epsilon=1+\sqrt{2}$. Hence $1+\sqrt{2}$ is the maximum value of ε, giving the following subradiant state:

$$|\mathrm{sr}\rangle_{N/2}=C_{N/2}\sum_{k=0}^{N/2}\frac{(-1/2\epsilon)^k}{k!}\sqrt{(2k)!}\left|\frac{N}{2}-k,2k,\frac{N}{2}-k\right\rangle. \tag{20}$$

For large N, the average value of k is $\langle k\rangle=1/4\epsilon=(\sqrt{2}-1)/4$, with variance $\sigma_k^2=\langle k\rangle$. From state (19) and the correspondence between p and ϵ, we may evaluate the average populations $P_i=\langle N_i\rangle/N$, with $i=0,1,2$, as a function of ε. The result is compared in Fig. 7 with semiclassical solutions (16) and (17), for $N=32$. We observe that the quantum solution does not show a sharp transition at $\varepsilon=1/\sqrt{3}$ as the classical one, but there is a tail which becomes negligible for $N\gg1$.

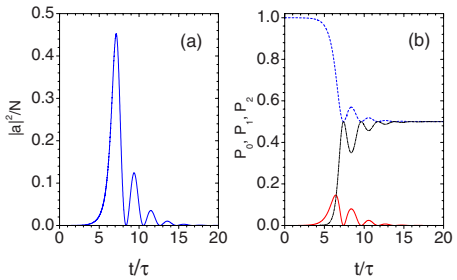

FIG. 5. (Color online) (a) Time evolution of the radiated intensity $|a|^2$ and the three populations P_0 (dashed blue line), P_1 (continuous red line), and P_2 (dashed-dotted black line) as functions of t/τ, where $\tau=(g\sqrt{N})^{-1}$, for the same parameters in Fig. 3 and $\epsilon=1+\sqrt{2}$.

B. Wigner function

Here we show the Wigner function of the subradiance state $|\mathrm{sr}\rangle$ in order to get some more properties of the system. We start from the definition

$$W(\alpha_0,\alpha_1,\alpha_2)=\int\prod_{i=0}^{2}\frac{d^2\xi_i}{\pi^2}e^{\xi_i^*\alpha_i-\alpha_i^*\xi_i}\chi(\xi_0,\xi_1,\xi_2), \tag{21}$$

where α_i and ξ_i are complex numbers and χ is the characteristic function defined as

$$\chi(\xi_0,\xi_1,\xi_2)=\langle\mathrm{sr}|\hat{D}_0(\xi_0)\hat{D}_1(\xi_1)\hat{D}_2(\xi_2)|\mathrm{sr}\rangle, \tag{22}$$

where $\hat{D}_j(\xi_j)=\exp(\xi_j\hat{c}_j^\dagger-\xi_j^*\hat{c}_j)$ is a displacement operator for the jth mode. A straightforward calculation, reported in the Appendix B, yields

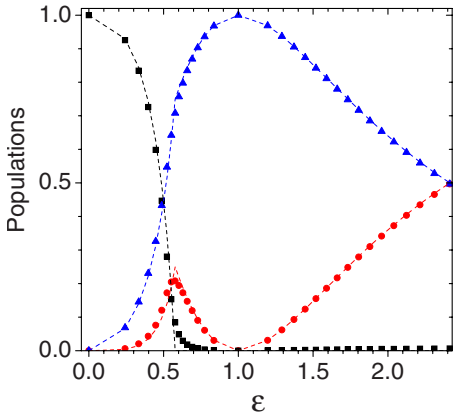

FIG. 7. (Color online) Quantum subradiance solution: population fractions of the three states, P_0 (red circles), P_1 (black squares), and P_2 (blue triangles) vs ϵ, obtained from Eq. (19) with $N=32$. The dashed lines show for comparison the semiclassical solution in Fig. 2.

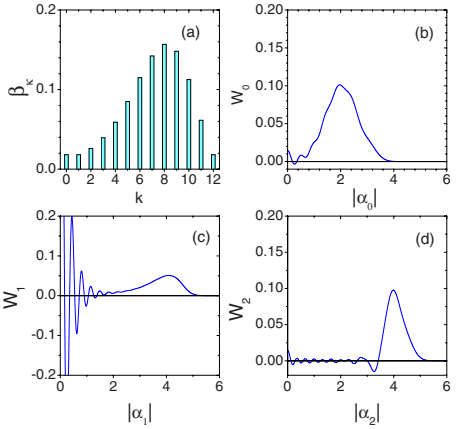

FIG. 8. (Color online) Subradiant state for $N=36$, $p=12$, and $\epsilon=1/2$: (a) probability β_k vs k; (b) W_0 vs $|\alpha_0|$; (c) W_1 vs $|\alpha_1|$; and (d) W_2 vs $|\alpha_2|$.

$$\chi(\xi_0,\xi_1,\xi_2) = e^{-(|\xi_0|^2+|\xi_1|^2+|\xi_2|^2)/2} \times \sum_{k=0}^{p} \beta_k L_{p-k}(|\xi_0|^2) L_{2k}(|\xi_1|^2) L_{N-p-k}(|\xi_2|^2), \tag{23}$$

and

$$W(\alpha_0,\alpha_1,\alpha_2) = \left(\frac{2}{\pi}\right)^3 e^{-2(|\alpha_0|^2+|\alpha_1|^2+|\alpha_2|^2)} \times \sum_{k=0}^{p} \beta_k L_{p-k}(4|\alpha_0|^2) L_{2k}(4|\alpha_1|^2) L_{N-p-k}(4|\alpha_2|^2), \tag{24}$$

where

$$\beta_k = C_p^2 \frac{(2k)!\,(N-p-k)!}{(p-k)!\,(k!)^2} \left(\frac{1}{2\epsilon}\right)^{2k} \tag{25}$$

and $L_n(x)$ is the Laguerre polynomial. Notice that the Wigner function depends only on the modulus of α_i and not from its phase. As expected, in general it is negative due to the presence of the Laguerre polynomials. By integrating over the other two-mode variables, from Eq. (24) we obtain the single-mode Wigner functions:

$$W(\alpha_0) = \frac{2}{\pi} e^{-2|\alpha_0|^2} \sum_{k=0}^{p} (-1)^{p-k} \beta_k L_{p-k}(4|\alpha_0|^2), \tag{26}$$

$$W(\alpha_1) = \frac{2}{\pi} e^{-2|\alpha_1|^2} \sum_{k=0}^{p} \beta_k L_{2k}(4|\alpha_1|^2), \tag{27}$$

$$W(\alpha_2) = \frac{2}{\pi} e^{-2|\alpha_2|^2} \sum_{k=0}^{p} (-1)^{N-p-k} \beta_k \times L_{N-p-k}(4|\alpha_2|^2). \tag{28}$$

In order to investigate the characteristics of the subradiance state, let us consider some specific examples. An interesting case is when $\epsilon=1/2$ and $p=N/3$, for which the semiclassical theory yields $P_0=1/9$ and $P_1=P_2=4/9$. Figure 8(a) shows the probability β_k vs k for $N=36$ and $p=12$. The probability is maximum for $k=8$, the average value is $\langle k\rangle=7.14$, and the standard deviation is $\sigma_k=2.64$. The single-mode Wigner functions $W_i=W(\alpha_i)$ are shown in Figs. 8(b)–8(d): W_0 has a maximum at $|\alpha_0|=2$ and W_1 and W_2 have a maximum at $|\alpha_1|=|\alpha_2|=4$, in agreement with the population values predicted by the semiclassical solution. However, W_1 differs considerably from W_2 with a strong oscillation near $|\alpha_1|=0$, probably due to the tail of the distribution at small k observed in Fig. 8(a). The single-mode Wigner functions present a pronounced maximum around which they are positive, plus an oscillating quantum background.

As a second example we consider the case $\epsilon=1+\sqrt{2}$, for which the semiclassical theory yields $P_1=0$ and $P_0=P_2=1/2$. In the quantum model it corresponds to the maximally antisymmetric state (20) with $p=N/2$. Figure 9(a) shows the probability β_k vs k for $N=36$ and $p=18$. The probability is maximum for $k=0$ and decreases rapidly to zero for larger k, with $\langle k\rangle=0.1$ and $\sigma_k=0.35$. The single-mode Wigner functions W_i are shown in Figs. 9(b)–9(d). W_0 and W_2 are equal and very similar to the Wigner function of the number state $|N/2\rangle$, $W(\alpha)=(4/\pi)\exp(-2|\alpha|^2)L_{N/2}(4|\alpha|^2)$ [21]. Furthermore, W_1 is equal to the vacuum Wigner function $W(\alpha)=(4/\pi)\exp(-2|\alpha|^2)$. In this case $N/2$ pairs of atoms with momentum 0 and $2\hbar q$ are produced.

Three-mode Wigner function (24), after integrating one-mode variable, yields the following two-mode Wigner functions:

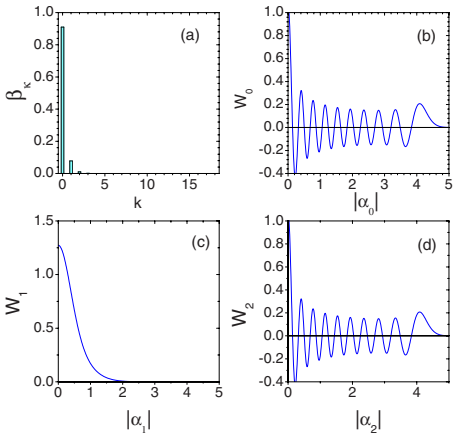

FIG. 9. (Color online) Subradiant state for $N=36$, $p=18$, and $\epsilon=1+\sqrt{2}$: (a) probability β_k vs k; (b) W_0 vs $|\alpha_0|$; (c) W_1 vs $|\alpha_1|$; and (d) W_2 vs $|\alpha_2|$.

$$W(\alpha_0,\alpha_1) = \left(\frac{2}{\pi}\right)^2 e^{-2(|\alpha_0|^2+|\alpha_1|^2)} \sum_{k=0}^{p} (-1)^{p+k} \beta_k L_{p-k}(4|\alpha_0|^2) L_{2k}(4|\alpha_1|^2), \tag{29}$$

$$W(\alpha_0,\alpha_2) = \left(\frac{2}{\pi}\right)^2 e^{-2(|\alpha_0|^2+|\alpha_2|^2)} \sum_{k=0}^{p} \beta_k L_{p-k}(4|\alpha_0|^2) L_{N-p-k}(4|\alpha_2|^2), \tag{30}$$

$$W(\alpha_1,\alpha_2) = \left(\frac{2}{\pi}\right)^2 e^{-2(|\alpha_1|^2+|\alpha_2|^2)} \sum_{k=0}^{p} (-1)^{p-k} \beta_k L_{p-k}(4|\alpha_1|^2) L_{2k}(4|\alpha_2|^2). \tag{31}$$

Figures 10–12 show the two-mode Wigner functions $W_{i,j}=W(\alpha_i,\alpha_j)$ as functions of $|\alpha_i|$ and $|\alpha_j|$, for $i,j=0,1,2$ and the case $N=36$ and $p=12$, corresponding to $\epsilon=1/2$ (see Fig. 8). The red color corresponds to a negative value of the functions. We observe several zones of negativity indicating nonclassical correlations between the two modes. In particular, $W_{0,1}$ and $W_{1,2}$ show strong correlations of modes 0 and 2 with mode 1, which has strong oscillations, whereas $W_{0,2}$ is larger near the vacuum value (0,0). Hence, we can say that qualitatively modes 0 and 2 behave quasiclassically, whereas mode 1 has features similar to a number state. Figure 13 shows $W_{0,2}$ vs $|\alpha_0|$ and $|\alpha_2|$ for the case $N=36$ and $p=18$, corresponding to $\epsilon=1+\sqrt{2}$ (see Fig. 9). The two-mode Wigner function looks like the product of two single-mode number Wigner functions shown in Figs. 9(b) and 9(d), with a bidimensional regular mesh of positive and negative zones.

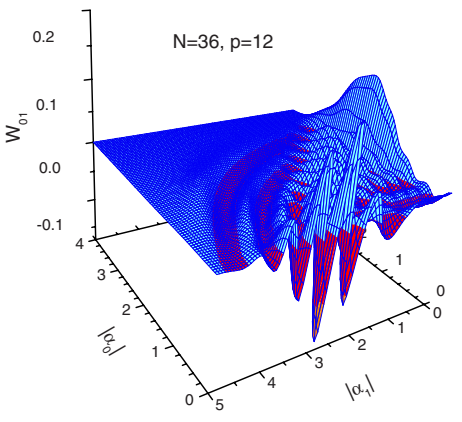

FIG. 10. (Color online) Two-mode Wigner function $W(\alpha_0,\alpha_1)$ for $N=36$, $p=12$. The red color corresponds to a negative value of the function.

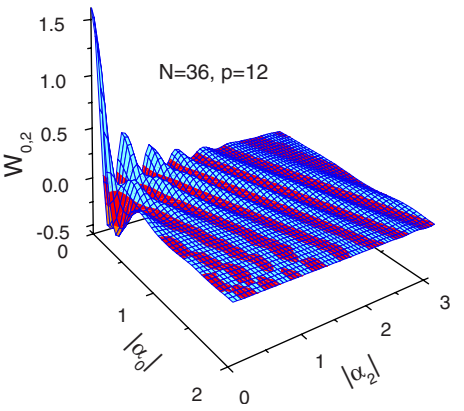

FIG. 11. (Color online) Two-mode Wigner function $W(\alpha_0,\alpha_2)$ for $N=36$, $p=12$.

C. Atom statistics

We calculate now the equal-time intensity correlation and cross-correlation functions, defined respectively as

$$g_i^{(2)}(0) = \frac{\langle \hat{c}_i^\dagger \hat{c}_i^\dagger \hat{c}_i \hat{c}_i \rangle}{\langle \hat{N}_i \rangle^2}, \tag{32}$$

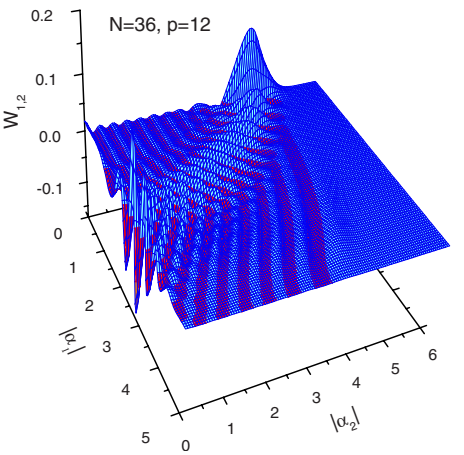

FIG. 12. (Color online) Two-mode Wigner function $W(\alpha_1,\alpha_2)$ for $N=36$, $p=12$.

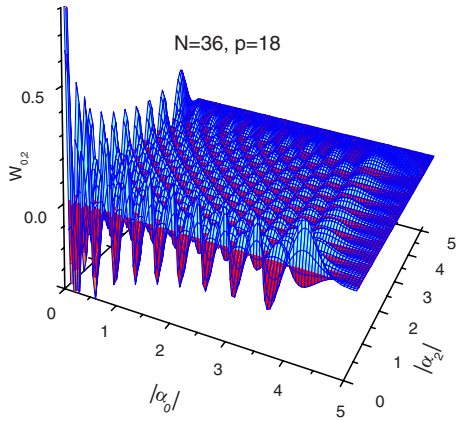

FIG. 13. (Color online) Two-mode Wigner function $W(\alpha_0,\alpha_2)$ for $N=36$, $p=18$.

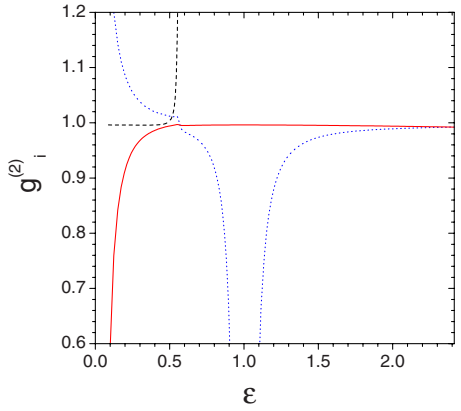

FIG. 14. (Color online) Intensity correlation functions vs ϵ: $g_0^{(2)}(0)$ (dotted blue line), $g_1^{(2)}(0)$ (dashed black line), and $g_2^{(2)}(0)$ (continuous red line).

$$g_{i,j}^{(2)}(0)=\frac{\langle\hat{N}_i\hat{N}_j\rangle}{\langle\hat{N}_i\rangle\langle\hat{N}_j\rangle}, \tag{33}$$

with $i=0,1,2$, $i\neq j$, and $\hat{N}_i=\hat{c}_i^\dagger\hat{c}_i$. For a classical field there is an upper limit to the second-order equal-time cross-correlation function given by the Cauchy-Schwartz inequality

$$g_{i,j}^{(2)}(0)\leq[g_i^{(2)}(0)g_j^{(2)}(0)]^{1/2}. \tag{34}$$

Quantum-mechanical fields, however, can violate this inequality and are instead constrained by

$$g_{i,j}^{(2)}(0)\leq\left[g_i^{(2)}(0)+\frac{1}{\langle\hat{N}_i\rangle}\right]^{1/2}\left[g_j^{(2)}(0)+\frac{1}{\langle\hat{N}_j\rangle}\right]^{1/2}, \tag{35}$$

which reduces to the classical results in the limit of large occupation numbers. We obtain the following expressions for the subradiant state:

$$g_0^{(2)}(0)=1+\frac{\sigma_k^2-\langle\hat{N}_0\rangle}{\langle\hat{N}_0\rangle^2}, \tag{36}$$

$$g_1^{(2)}(0)=1+\frac{4\sigma_k^2-\langle\hat{N}_1\rangle}{\langle\hat{N}_1\rangle^2}, \tag{37}$$

$$g_2^{(2)}(0)=1+\frac{\sigma_k^2-\langle\hat{N}_2\rangle}{\langle\hat{N}_2\rangle^2}, \tag{38}$$

where $\sigma_k^2=\langle k^2\rangle-\langle k\rangle^2$ and

$$\langle k^m\rangle=\sum_{k=0}^{p}k^m\beta_k.$$

The cross-correlation functions are

$$g_{0,1}^{(2)}(0)=1-\frac{2\sigma_k^2}{\langle\hat{N}_0\rangle\langle\hat{N}_1\rangle}, \tag{39}$$

$$g_{0,2}^{(2)}(0)=1+\frac{\sigma_k^2}{\langle\hat{N}_0\rangle\langle\hat{N}_2\rangle}, \tag{40}$$

$$g_{1,2}^{(2)}(0)=1-\frac{2\sigma_k^2}{\langle\hat{N}_1\rangle\langle\hat{N}_2\rangle}. \tag{41}$$

From Eqs. (36)–(41) it follows that

$$g_{0,1}^{(2)}(0)^2=\left(g_0^{(0)}(0)+\frac{1}{\langle\hat{N}_0\rangle}\right)\left(g_1^{(2)}(0)+\frac{1}{\langle\hat{N}_1\rangle}\right)-\sigma^2\left(\frac{1}{\langle\hat{N}_0\rangle}+\frac{2}{\langle\hat{N}_1\rangle}\right)^2, \tag{42}$$

$$g_{0,2}^{(2)}(0)^2=\left(g_0^{(0)}(0)+\frac{1}{\langle\hat{N}_0\rangle}\right)\left(g_2^{(2)}(0)+\frac{1}{\langle\hat{N}_2\rangle}\right)-\sigma^2\left(\frac{1}{\langle\hat{N}_0\rangle}-\frac{1}{\langle\hat{N}_2\rangle}\right)^2, \tag{43}$$

$$g_{1,2}^{(2)}(0)^2=\left(g_1^{(2)}(0)+\frac{1}{\langle\hat{N}_1\rangle}\right)\left(g_2^{(2)}(0)+\frac{1}{\langle\hat{N}_2\rangle}\right)-\sigma^2\left(\frac{2}{\langle\hat{N}_1\rangle}+\frac{1}{\langle\hat{N}_2\rangle}\right), \tag{44}$$

showing that $g_{ij}^{(2)}(0)$ are consistent with quantum inequality (35). Figure 14 shows the intensity correlation functions $g_i^{(2)}(0)$ for $i=0,1,2$, for subradiance state (19). We obtain that $g_2^{(2)}(0)$ (continuous red line) is less than unity for all the values of ϵ and $g_0^{(2)}(0)$ (dotted blue line) is less than unity for $\epsilon>1/\sqrt{3}$. So antibunching occurs for the momentum states $m=0$ and $m=2$, but not for the state $m=1$.

Figures 15–17 show the eventual violation of Cauchy-Schwartz inequality (34) for $g_{i,j}^{(2)}$ (continuous red line). The dashed black line is the classical upper limit $[g_i^{(2)}(0)g_j^{(2)}(0)]^{1/2}$ and the dotted blue line is the quantum upper limit $\{[g_i^{(2)}(0)+1/\langle\hat{N}_i\rangle][g_j^{(2)}(0)+1/\langle\hat{N}_j\rangle]\}^{1/2}$. We found that $g_{0,1}^{(2)}$ is always consistent with the classical inequality,

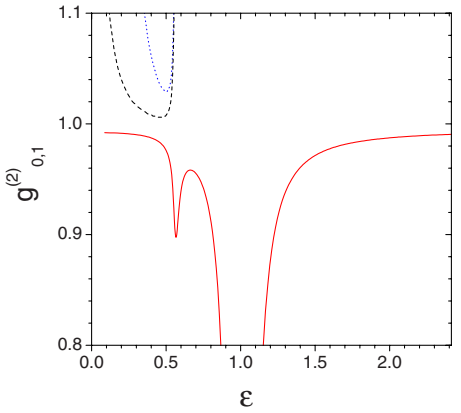

FIG. 15. (Color online) Cross-correlation function $g^{(2)}_{0,1}(0)$ (continuous red line) vs ϵ. The dashed black line indicates the classical upper limit of inequality (34); the dotted blue line indicates the quantum upper limit of inequality (35).

whereas $g^{(2)}_{0,2}$ and $g^{(2)}_{1,2}$ violate Cauchy-Schwartz inequality (34) for all the ε and for $\epsilon<0.47$, respectively, showing the existence of quantum correlations between the modes $m=0$ and $m=2$ and between the modes $m=1$ and $m=2$. For $\epsilon>1/\sqrt{3}$, $g^{(2)}_{0,2}$ is close to the upper limit of quantum inequality (35).

D. Entanglement

Subradiant state (19) is a tripartite pure state. Unfortunately it is difficult to evaluate entanglement for tripartite non-Gaussian states, even if they are pure. On the other hand, it is known that the von Neumann entropy is a good measure of entanglement for bipartite pure states [22]. If we consider the one-mode reduced density operators $\rho_i=\mathrm{Tr}_{jk}[\rho_{ijk}]$ (for each $i\neq j\neq k$) obtained tracing on the other two modes, the associated von Neumann entropy is $S[\rho_i]=-\Sigma_{k=0}^{p}\beta_k\ln(\beta_k)$. Due to the particular form of subradiant state (19), $S[\rho_1]=S[\rho_2]=S[\rho_3]$. As shown in [22], if the entropy $S[\rho_i]$ is positive then the i mode is entangled to the (j,k) pair taken as a whole. The one-mode entropy $S[\rho_i]$ is shown in Fig. 18 vs the two-pump field amplitude ratio ε. It is always positive unless for $\epsilon=0$ and $\epsilon=1$, when the state reduces to $|0,N,0\rangle$ and $|0,0,N\rangle$, respectively. Moreover, it has a maximum for $\epsilon=1/\sqrt{3}$.

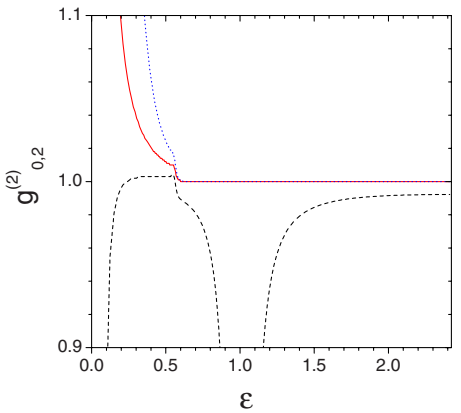

FIG. 16. (Color online) Same as in Fig. 15 but for $g^{(2)}_{0,2}(0)$.

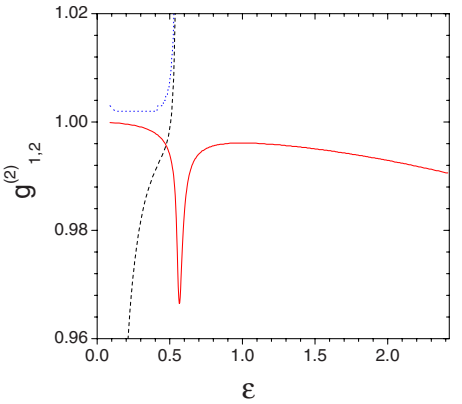

FIG. 17. (Color online) Same as in Fig. 15 but for $g^{(2)}_{1,2}(0)$.

IV. CONCLUSIONS

We have investigated a possible way to observe subradiance with ultracold atoms in a high-finesse ring cavity, scattering photons from a two-frequency pump laser into a single-frequency cavity mode via the QCARL mechanism. Subradiance occurs in a degenerate cascade between three motional levels separated by the two-photon momentum recoil $\hbar\vec{q}$, where $\vec{q}=\vec{k}-\vec{k}_s$ is the momentum transfer between the pump and the cavity modes. The observation of subradiance in momentum transitions of cold atomic samples presents several advantages and differences with respect to the electronic transitions of excited two-level atoms. First, the momentum transitions are not affected by the spontaneous emission if the pump laser is sufficiently detuned from the atomic resonance. Second, the atomic condensates have a long life and a very long coherence time, allowing the preparation and the further manipulation of the subradiant state. Third, the subradiance is realized among collective motional states containing a large number of atoms. Subradiance as well super-radiance does not require that the dimension of the sample be smaller than the radiation wavelength, as in

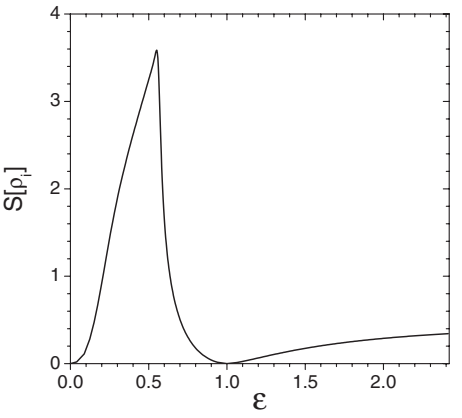

FIG. 18. One-mode entropy $S[\rho_i]$ vs the two-pump field amplitude ratio ϵ, for $N=256$.

super-radiance by excited atoms. For these reasons, subradiance between motional states of ultracold atoms may be important for the study of the decoherence-free subspaces sought in quantum information [23]. Other recent proposals of realizing subradiance in matter wave require a very fine control of single atoms in optical cavities [24], which can be very problematic experimentally. On the other hand, the experimental activity on super-radiant Rayleigh scattering and CARL with Bose-Einstein condensates [1,25] has achieved important progress and a subradiance experiment with BEC in a ring cavity could be feasible with the present techniques. At ultracold temperature and with a coupling constant $g\sqrt{N}$ much less than the recoil frequency ω_r, it should be possible (using a two-frequency laser with frequency difference of $2\omega_r$) to restrict the momentum transitions up to involve only the first two recoil momentum states. Recent experiments on super-radiant scattering from a BEC pumped by a two-frequency laser beam [26,27] have shown that the momentum transitions are enhanced by the presence of the second pump detuned by $2\omega_r$. However, only by inserting the BEC in a high-finesse ring cavity will it be possible to limit the transition sequence. Then, varying the relative intensity of the two pump laser beams should be possible to probe the transition from super-radiance to subradiance. As an example of possible experimental parameters, subradiance could be observed in a ring cavity similar to that realized in Tübingen [28] (with length $L=87$ mm, beam waist $w=100$ μm, and finesse $F=5\times10^5$, about five times the presently achieved value) with $\kappa=0.2\omega_r$ and $g\sqrt{N}=0.2\omega_r$. This last value can be obtained using a ^{87}Rb condensate [with $\omega_r=(2\pi)15$ kHz] with $N=10^4$ atoms at a temperature of some tens of nK, driven by two laser beams with $P_0=174$ mW, $\Delta_0=-(2\pi)3$ THz, and a frequency difference precision of $\delta\omega\leq5$ kHz. Subradiance will be reached in about 100μs, less than the decoherence time of the BEC.

ACKNOWLEDGMENTS

We thank M. G. A. Paris and S. Olivares for enlightening discussions about entanglement.

APPENDIX A: THE SUBRADIANCE STATE

In order to demonstrate Eq. (19) let us consider a state of the form

$$|\mathrm{sr}\rangle=\sum_{n_1=0}^{N}\sum_{(n_0,n_2)}f(n_0,n_2)|n_0,n_1,n_2\rangle,$$

where the second sum is over all the pairs (n_0,n_2) such that $n_0+n_2=N-n_1$. When substituted into Eq. (18), it yields

$$\sum_{n_1=0}^{N-1}\sum_{(n_0,n_2),n_0\neq0}f(n_0,n_2)\sqrt{n_0(n_1+1)}|n_0-1,n_1+1,n_2\rangle+\epsilon\sum_{n_1=1}^{N}\sum_{(n_0,n_2),n_2\neq N}f(n_0,n_2)\sqrt{n_1(n_2+1)}|n_0,n_1-1,n_2+1\rangle=0. \tag{A1}$$

After having redefined the indices n_1 and n_2 in the sums, it becomes

$$\left\{\sum_{n_1=1}^{N}\sum_{\substack{(n_0,n_2)\\n_0\neq N}}f(n_0+1,n_2)\sqrt{(n_0+1)n_1}+\epsilon\sum_{n_1=0}^{N-1}\sum_{\substack{(n_0,n_2)\\n_2\neq0}}f(n_0,n_2-1)\sqrt{(n_1+1)n_2}\right\}|n_0,n_1,n_2\rangle=0. \tag{A2}$$

The terms in the curly brackets of Eq. (A2) vanish when the following conditions are met:

(1) In the second sum on n_1 in the curly brackets the term with $n_1=N$ is missing: since in the first sum $n_0=n_2=0$ when $n_1=N$, it yields $f(1,0)=0$.

(2) In the first sum on n_1 in the curly brackets the term with $n_1=0$ is missing: then the second sum on n_1 with $n_1=0$, $n_2=N-n_0$, and $n_2\neq0$ yields

$$f(n_0,N-n_0-1)=0,\quad n_0=0,\ldots,N-1. \tag{A3}$$

(3) The remaining sum in Eq. (A2)yields

$$\sum_{(n_0,n_2)}f(n_0+1,n_2)\sqrt{(n_0+1)n_1}+\epsilon\sum_{(n_0,n_2),n_2\neq0}f(n_0,n_2-1)\sqrt{(n_1+1)n_2}=0, \tag{A4}$$

with $n_1=1,\ldots,N-1$. In the second sum of Eq. (A2) the term $n_2=0$ is missing, so in the first sum the term with $n_2=0$ and $n_0=N-n_1$ vanishes and yields $f(k,0)=0$ with $k=2,\ldots,N$. Together with the result of item 1, it yields

$$f(k,0)=0,\quad k=1,2,\ldots,N \tag{A5}$$

whereas the remaining terms of Eq. (A4) yield

$$\sqrt{(n_0+1)n_1}f(n_0+1,N-n_0-n_1)=-\epsilon\sqrt{(n_1+1)(N-n_0-n_1)}f(n_0,N-n_0-n_1-1), \tag{A6}$$

with $n_1=1,\ldots,N-1$ and $n_0=0,\ldots,N-n_1$.

For $n_1=2$ Eq. (A6) yields

$$\sqrt{2(n_0+1)}f(n_0+1,N-n_0-2)=-\epsilon\sqrt{3(N-n_0-3)}f(n_0,N-n_0-3),\quad n_0=0,\ldots,N-3. \tag{A7}$$

Since from Eq. (A3) $f(n_0+1,N-n_0-2)=0$, then

$$f(n_0,N-n_0-3)=0,\quad n_0=0\ldots,N-3. \tag{A8}$$

Continuing with all the even values of n_1, it is easy to show that

$$f(n_0,N-n_0-k)=0,\quad k=1,3,\ldots,N-n_0\ \text{(odd)},\qquad n_0=0\ldots,N-k. \tag{A9}$$

Hence, the only terms different from zero are those with $n_1=2q+1$ and $q=0,\ldots,N/2-1$, yielding

$$f(n_0+1,N-n_0-2q-1) = -\epsilon\sqrt{\frac{(2q+2)(N-n_0-2q-1)}{(n_0+1)(2q+1)}}f(n_0,N-n_0-2q-2), \tag{A10}$$

where $n_0=0,\ldots,N-(2q+1)$. Equation (A10) provides a recurrence relation for the index n_0 with a given n_0+q. In fact the difference between the first and second indices of $f(a,b)$ in both the left and right terms of Eq. (A10) is $\Delta=b-a=N-2(n_0+q+1)$. So, introducing the new index $p=n_0+q+1$, Eq. (A10) can be written, for $p=1,\ldots,N/2$, as

$$f(p-q-1,N-p-q-1) = -\frac{1}{\epsilon}\sqrt{\frac{(2q+1)(p-q)}{(2q+2)(N-p-q)}}f(p-q,N-p-q), \quad q=0,\ldots,p. \tag{A11}$$

By iteration of Eq. (A11) we obtain

$$f(p-q,N-p-q) = \left(-\frac{1}{\epsilon}\right)^q\sqrt{\frac{(2q+1)!!}{(2q)!!}\frac{p!\,(N-p-q)!}{(p-q)!\,(N-p)!}} \times f(p,N-p), \quad q=0,\ldots,p, \tag{A12}$$

where $(2k)!!=2k(2k-2)\cdots2\times1$ and $(2k+1)!!=(2k+1)(2k-1)\cdots3\times1$. Since $(2q+1)!!/(2q)!!=(2q)!/(2^q q!)^2$, finally we obtain

$$|\mathrm{sr}\rangle = C_p\sum_{q=0}^{p}\left(-\frac{1}{2\epsilon}\right)^q \times\sqrt{\frac{(2q)!\,(N-p-q)!}{(q!)^2(p-q)!}}|p-q,2q,N-p-q\rangle, \tag{A13}$$

where $C_p=[p!/(N-p)!]^{1/2}f(p,N-p)$.

APPENDIX B: DERIVATION OF THE SUBRADIANT WIGNER FUNCTION

We demonstrate Eq. (23). Writing the displacement operator as a product of operators, $\hat{D}(\xi)=\exp(-|\xi|^2/2)\exp(\xi\hat{c}^\dagger)\exp(-\xi^*\hat{c})$, and using the formula

$$\exp(-\xi^*\hat{c})|k\rangle = \sum_{n=0}^{k}\frac{(-\xi^*)^n}{n!}\sqrt{\frac{k!}{(k-n)!}}|k-n\rangle,$$

we obtain

$$\langle k'|\hat{D}(\xi)|k\rangle = e^{-|\xi|^2/2}L_k(|\xi|^2)\delta_{k,k'}, \tag{B1}$$

where

$$L_k(x) = \sum_{n=0}^{k}(-1)^n\binom{k}{n}\frac{x^n}{n!}$$

is the Laguerre polynomial of order k. Using Eq. (B1) in Eq. (22) with subradiant state (19) we obtain

$$\chi(\xi_0,\xi_1,\xi_2) = e^{-(|\xi_0|^2+|\xi_1|^2+|\xi_2|^2)/2} \times\sum_{k=0}^{p}\beta_k L_{p-k}(|\xi_0|^2)L_{2k}(|\xi_1|^2)L_{N-p-k}(|\xi_2|^2). \tag{B2}$$

In order to evaluate Wigner function (21) we must calculate an integral of the form

$$I_m(\alpha) = \int d^2\xi e^{\xi^*\alpha-\alpha^*\xi-|\xi|^2/2}L_m(|\xi|^2). \tag{B3}$$

Introducing polar coordinates $\xi=-ir\exp(i\phi)$ and $\alpha=|\alpha|\exp(i\psi)$ it transforms into

$$I_m(\alpha) = \int_0^\infty dr\, re^{-r^2/2}L_m(r^2)\int_0^{2\pi}d\phi e^{2ir|\alpha|\cos(\phi-\psi)} = 2\pi\int_0^\infty dr\, re^{-r^2/2}L_m(r^2)J_0(2r|\alpha|), \tag{B4}$$

where $J_0(x)$ is the Bessel function of zero order. Using the formula [29]

$$\int_0^\infty dx\, xe^{-ax^2/2}L_n(bx^2/2)J_0(xy) = \frac{(a-b)^n}{a^{n+1}}e^{-y^2/2a}L_n\left(\frac{by^2}{2a(b-a)}\right), \tag{B5}$$

we obtain

$$I_m(\alpha) = 2\pi(-1)^m e^{-2|\alpha|^2}L_m(4|\alpha|^2). \tag{B6}$$

So, from the definition of Wigner function (21) and using Eqs. (B2) and (B6), we obtain

$$W(\alpha_0,\alpha_1,\alpha_2) = \frac{1}{\pi^6}\sum_{k=0}^{p}\beta_k I_{p-k}(\alpha_0)I_{2k}(\alpha_1)I_{N-p-k}(\alpha_2), \tag{B7}$$

which coincides with Eq. (24). Using the formula [29]

$$\int_0^\infty dx\, e^{-x/a}L_m(x) = a(1-a)^n, \tag{B8}$$

we have

$$\frac{1}{\pi^2}\int d^2\alpha I_m(\alpha) = 1. \tag{B9}$$

From Eqs. (B6), (B7), and (B9) we obtain expressions (26)–(31) of the one-mode and two-mode reduced Wigner functions, respectively.

[1] S. Inouye, A. P. Chikkatur, D. M. Stamper-Kurn, J. Stenger, D. E. Pritchard, and W. Ketterle, Science **285**, 571 (1999).
[2] S. Inouye, T. Pfau, S. Gupta, A. P. Chikkatur, A. Görlitz, D. E. Pritchard, and W. Ketterle, Nature (London) **402**, 641 (1999).
[3] M. Kozuma, Y. Suzuki, Y. Torii, T. Sugiura, T. Kugam, E. W. Hagley, and L. Deng, Science **286**, 2309 (1999).
[4] L. Fallani, C. Fort, N. Piovella, M. M. Cola, F. S. Cataliotti, M. Inguscio, and R. Bonifacio, Phys. Rev. A **71**, 033612 (2005).
[5] D. Schneble, G. K. Campbell, E. W. Streed, M. Boyd, D. E. Pritchard, and W. Ketterle, Phys. Rev. A **69**, 041601(R) (2004).
[6] Y. Yoshikawa, T. Sugiura, Y. Torii, and T. Kuga, Phys. Rev. A **69**, 041603(R) (2004).
[7] M. Gross and S. Haroche, Phys. Rep. **93**, 301 (1982).
[8] N. Piovella, M. Gatelli, and R. Bonifacio, Opt. Commun. **194**, 167 (2001).
[9] G. R. M. Robb, N. Piovella, and R. Bonifacio, J. Opt. B: Quantum Semiclassical Opt. **7**, 93 (2005).
[10] N. Piovella, M. Gatelli, L. Martinucci, R. Bonifacio, B. W. J. McNeil, and G. R. M. Robb, Laser Phys. **12**, 188 (2003).
[11] R. Bonifacio and L. De Salvo Souza, Nucl. Instrum. Methods Phys. Res. A **341**, 360 (1994).
[12] R. Bonifacio, L. De Salvo, L. M. Narducci, and E. J. D'Angelo, Phys. Rev. A **50**, 1716 (1994).
[13] R. H. Dicke, Phys. Rev. **93**, 99 (1954).
[14] D. Pavolini, A. Crubellier, P. Pillet, L. Cabaret, and S. Liberman, Phys. Rev. Lett. **54**, 1917 (1985).
[15] A. Crubellier, S. Liberman, D. Pavolini, and P. Pillet, J. Phys. B **18**, 3811 (1985).
[16] A. Crubellier and D. Pavolini, J. Phys. B **19**, 2109 (1986).
[17] A. Crubellier, J. Phys. B **20**, 971 (1987).
[18] A. Crubellier and D. Pavolini, J. Phys. B **20**, 1451 (1987).
[19] M. M. Cola, L. Volpe, and N. Piovella, Phys. Rev. A **79**, 013613 (2009).
[20] N. Piovella, M. M. Cola, and R. Bonifacio, Phys. Rev. A **67**, 013817 (2003).
[21] D. F. Walls and G. J. Milburn, *Quantum Optics* (Springer, Berlin, 1994), p. 64.
[22] S. M. Barnett and S. J. D. Phoenix, Phys. Rev. A **44**, 535 (1991).
[23] D. A. Lidar, I. L. Chuang, and K. B. Whaley, Phys. Rev. Lett. **81**, 2594 (1998).
[24] P. Földi, M. G. Benedict, and A. Czirják, Phys. Rev. A **65**, 021802(R) (2002).
[25] S. Slama, S. Bux, G. Krenz, C. Zimmermann, and Ph. W. Courteille, Phys. Rev. Lett. **98**, 053603 (2007).
[26] N. Bar-Gill, E. E. Rowen, and N. Davidson, Phys. Rev. A **76**, 043603 (2007).
[27] F. Yang, X. Zhou, J. Li, Y. Chen, L. Xia, and X. Chen, Phys. Rev. A **78**, 043611 (2008).
[28] S. Slama, G. Krenz, S. Bux, C. Zimmermann, and Ph. W. Courteille, Phys. Rev. A **75**, 063620 (2007).
[29] I. S. Gradshteyn and I. M. Ryzhuk, *Table of Integrals, Series and Products* (Academic, San Diego, 2000), pp. 803–805.